SUPPLEMENTARY FIGURES

A

Focal section

0°

20 μm

B

Emission line profile

10 μm

VF readout

Soma

Tissue volume fraction, %

C

Volume fraction (%)

Cntrl Carbenoxolon

D

- control
- HFS (LTP)
- LFS (LTD)

fEPSP slope (% of baseline)

Time (min)

VF (% of baseline)

Time (min)

E

Astrocyte VF (% baseline)

ctrl LTP LTD

F

G

R = -0.47
p < 0.0001

Segmentation (S)

Average cross-section (μm²)

H

Segmentation (S)

R = 0.78
p < 0.0001

Number of processes

I

Hyper

APV Ca²⁺ clamp

no HFS

LTP

Hypo

Segmentation (%)

Volume fraction (%)

J

Image entropy

- Simulations
- Experiments

Volume fraction (%)

K

Hypo
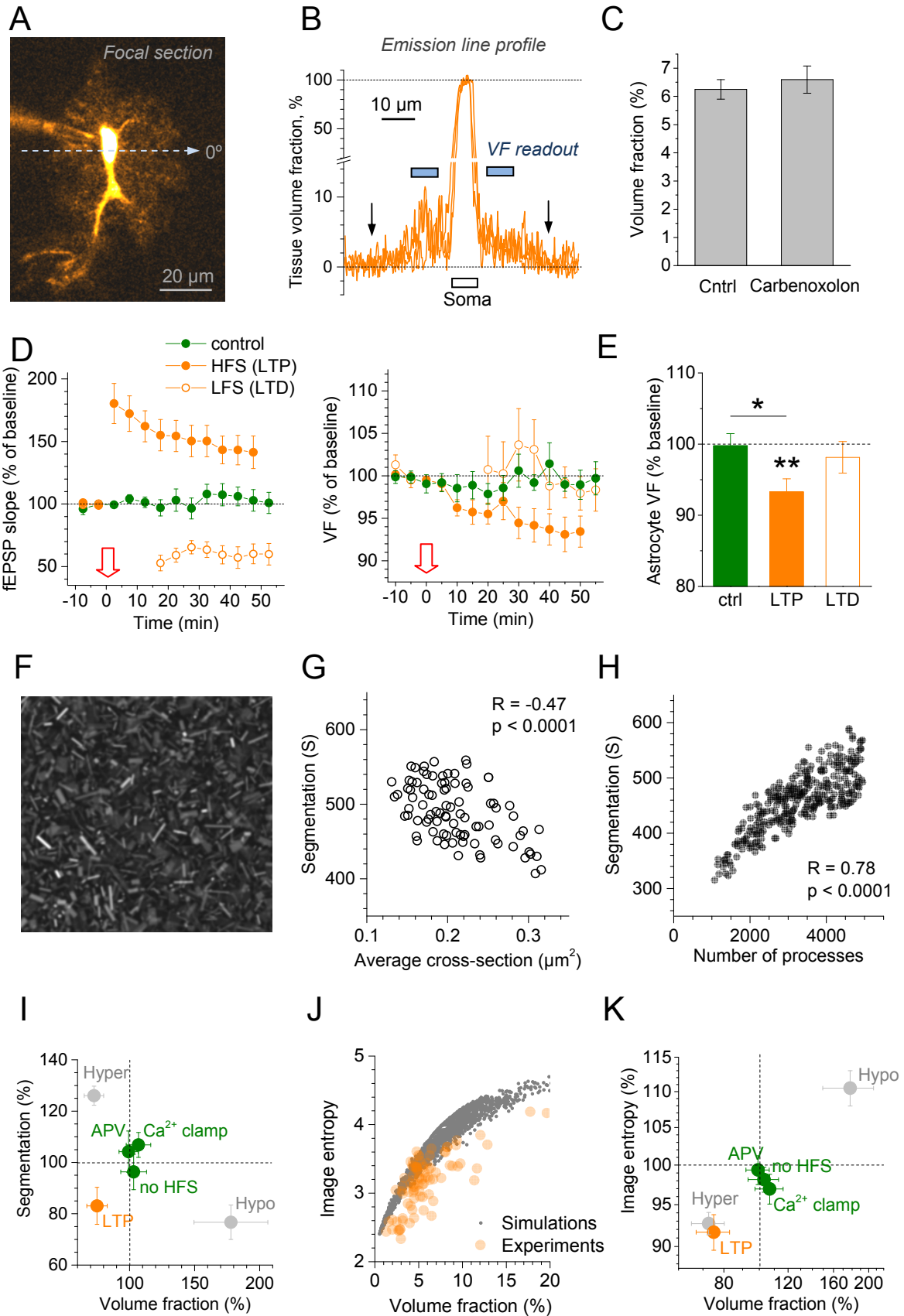
APV no HFS

Hyper Ca²⁺ clamp

LTP

Image entropy (%)

Volume fraction (%)

1

Figure S1. Astroglial tissue volume fraction (VF) monitored with independent imaging methods during the induction of LTP. Related to Fig. 1.

(A) CA1 astrocyte, single 2PE-section image (λ_x^{2p} = 800 nm; Alexa Fluor 594 hydrazide; 50 µM gap-junction blocker carbenoxolone); dashed line, line readout of emission intensity profile (an example crossing the soma; angle 0º; false color scale).

(B) Example of three astrocyte fluorescence profiles (measured using the original 16-bit grey-level image, background-corrected): along the line illustrated in A (0º), at 45º, and 135º. Data normalized to the emission intensity within the soma; arrows, detectable edges of the astrocyte profile; blue segments, typical ROI position for averaging VF readout during LTP induction (as shown in Fig. 1B): this region was routinely chosen to avoid thick primary processes near the soma as well as the uneven edges of the astroglial tree towards its periphery

(C) Average VF values for the astrocyte arbors in control conditions (mean ± SEM: 6.2 ± 0.35 %, n = 83) were not statistically different from those obtained in the presence of gap junction blocker carbenoxolone (6.6 ± 0.48%, n = 17, p = 0.56, unpaired Student's t-test).

(D) Monitoring fEPSCs (left) and astroglial VF change (right) in astroglia (mean ± SEM) expressing cytosolic EGFP under a human GFAP promoter (hGFAP-EGFP) (Nolte et al., 2001); in control conditions (green dots, n = 6), during HFS LTP induction (solid orange circles; red arrow, onset; n = 13), and during the induction LTD (low-frequency induction protocol, 1800 stimuli at 2 Hz; red arrow, onset).

(E) Statistical summary for VF changes in experiments shown in (D). VF was reduced after LTP induction by 7 ± 2 % (n = 13, ** p < 0.004) but not in control condition (+0.23 ± 1.7 %, n = 6, difference with LTP at *p = 0.021). LTD induction had no effect on VF (change -1.9 ± 2.2 %, n = 7, p = 0.43). Note that detected VF changes in EGFP-expressing cells underestimate the effect because diffusion equilibration of EGFP is much slower than that of Alexa Fluor (MW are 33 kDa and 760 Da, respectively): thus, upon cell shrinkage the decrease in the local EGFP fluorescence (which reports VF) is likely to be substantially retarded.

(F) An illustration of **c**omputer simulations mimicking 3D multi-segment structures (akin to astrocyte processes) imaged in a focal 2PE plane (Methods Details). The example depicts a simulated optical section containing 4042 astrocyte processes with an average visible size (0.2 µm x 1 µm x 1 µm) roughly reproducing EM observations (giving an average process volume of 0.20 μm^3). Here, ~9% of the simulated volume is occupied by simulated astrocyte processes, consistent with the experimental values.

(G) Testing Segmentation measure on simulated geometries: The maximum number of detectable particles in the image (Segmentation, see Method Details) decreases as the average process cross-section (hence volume) increases ~3-fold, from 0.13 to 0.33 μm^3 (4000-4500 astrocyte processes, n = 89 runs).

(H) Segmentation increases with the increasing number of simulated astrocyte processes (1000-5000 range) which have an average volume fraction of 0.18-0.24 µm^3 (*n* = 297).

(I) A summary of the relationships between VF and segmentation across experimental scenarios (mean ± SEM; data samples as shown in Fig. 1F and H). Average VF and segmentation under osmotic challenge report net cell volume changes. Results during LTP are more complex: they are best explained by having fewer and possibly smaller PAPs, because a straightforward PAP volume reduction would increase segmentation (G).

(J) Image entropy (Method Details) changes shown in register with astrocyte VF in simulated astrocyte process imaging and experimental data (simulations, *n* = 1736, Spearman rank test, R = 0.97, *P* < 0.0001, experimental data, *n* = 83, Spearman rank test, R = 0.69, *P* < 0.0001). In contrast to VF, entropy measurements do not require normalization to somatic fluorescence intensities and thus provides an independent (albeit qualitative) estimate of VF changes.

(K) Image entropy follows astrocyte VF across experimental scenarios, in response to LTP-induction and osmolarity changes (experimental samples as in I). The data support image entropy as an image intensity-independent reporter of VF.
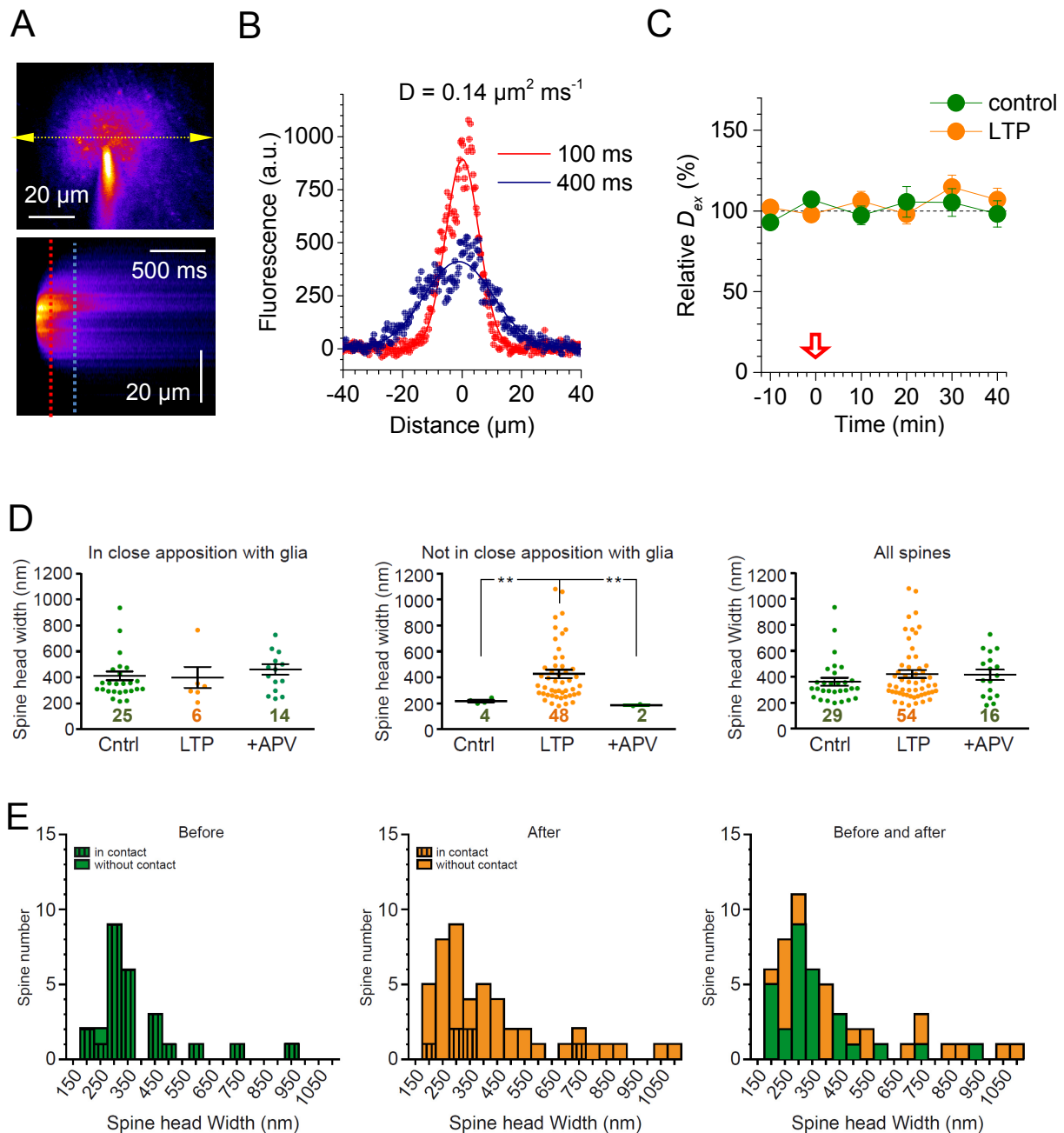
Figure S2. Extracellular diffusivity and super-resolution probing of LTP-associated changes in astroglial environment. Related to Fig. 2.

(A) Measuring local extracellular diffusivity. *Top:* A snapshot of a pressurized pipette filled with Alexa Fluor 594 and placed in CA1 *s. radiatum* area near recorded astroglia; arrows, linescan position near the pipette tip. *Bottom*: Example of a linescan recording of a brief (2-6 ms) pulse ejection of the dye; dashed lines, sampling of the extracellular fluorescence intensity (effective dye concentration) profiles at 100 ms and 400 ms post-pulse (Zheng et al., 2008).

(B) Fluorescence intensity (effective dye concentration) profiles (as in A) approximated with a Gaussian function, as detailed earlier, colors correspond to lines in A. Effective

extracellular diffusion coefficient (indicated) is obtained by analyzing the time evolution of such profiles, as described earlier (Zheng et al., 2008).

(C) Time course of the extracellular diffusivity in experiments with and without LTP induction (arrow), as indicated; average extracellular diffusivity 40 minutes after LTP induction was $107.0 \pm 7.1\%$ of baseline ($n = 8$), at a similar time point in control (no-LTP) experiments was $98.2 \pm 8.2\%$ of baseline ($n = 6$).

(D) Effects of LTP induction on the occurrence of close astroglia-spine apposition and on the dendritic spine head sizes monitored with STED microscopy. Digits show the numbers of identified spine heads under pseudo-random inspection of the area of interest. Mean ± SEM values are shown; LTP, data 25 min after LTP induction; +APV, 25 min after LTP induction protocol applied in the presence of 50 µM APV; ** $p < 0.01$ (Kruskall-Wallis ANOVA, sample sizes n are shown).
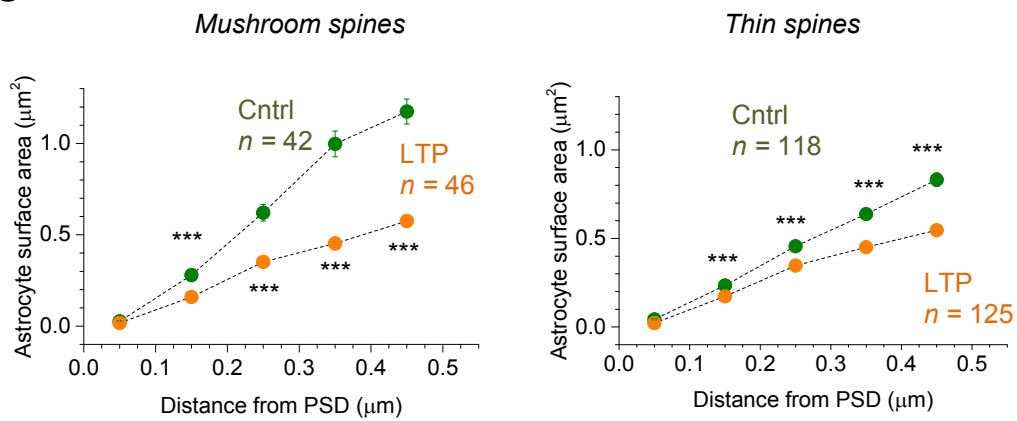
(E) Frequency histograms of spine head sizes before and 20-25 min after the induction of LTP (data set as in D), also with the separation between spines which are closely approached (striped columns) and not approached (plain columns) by astroglial processes, as indicated.

A
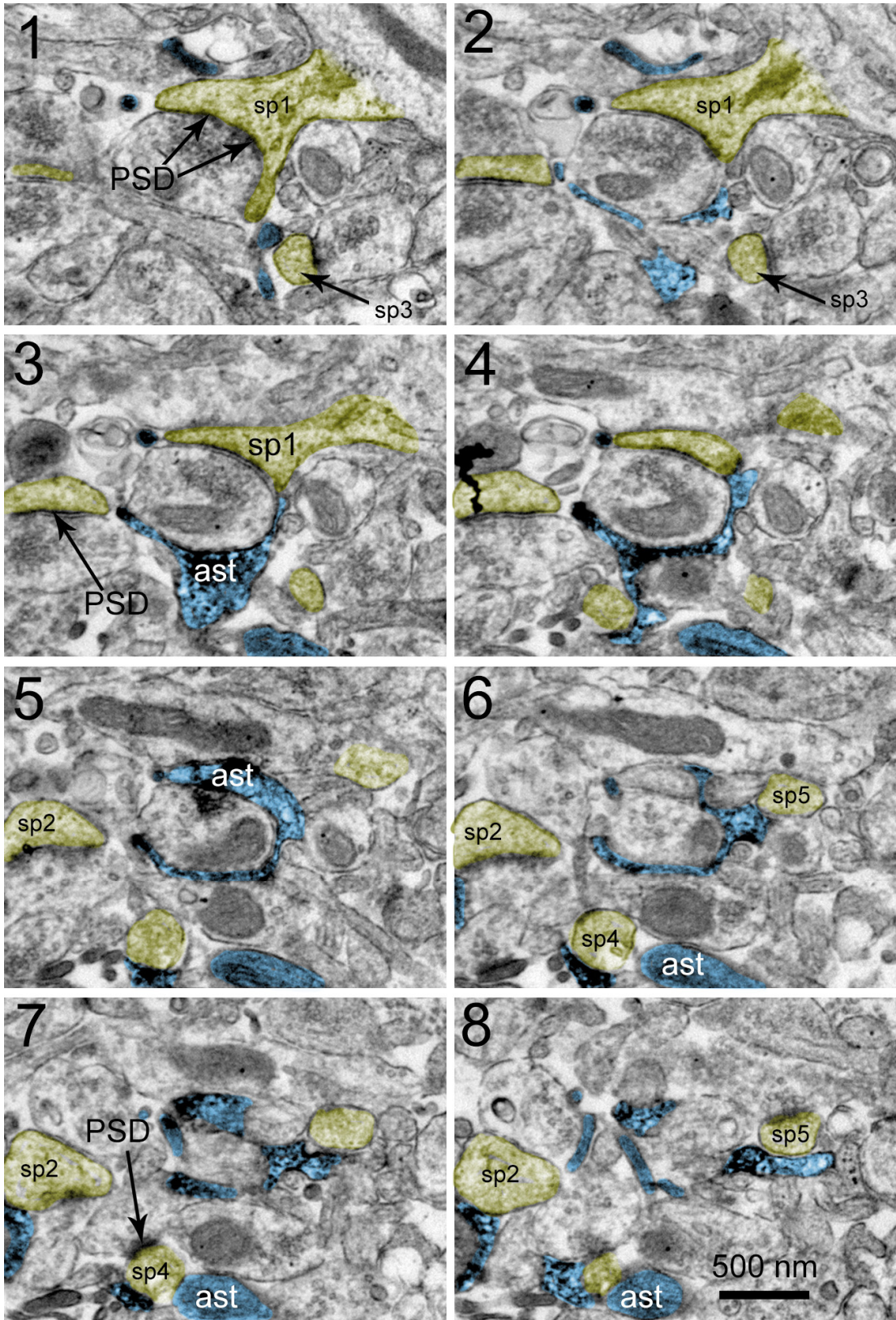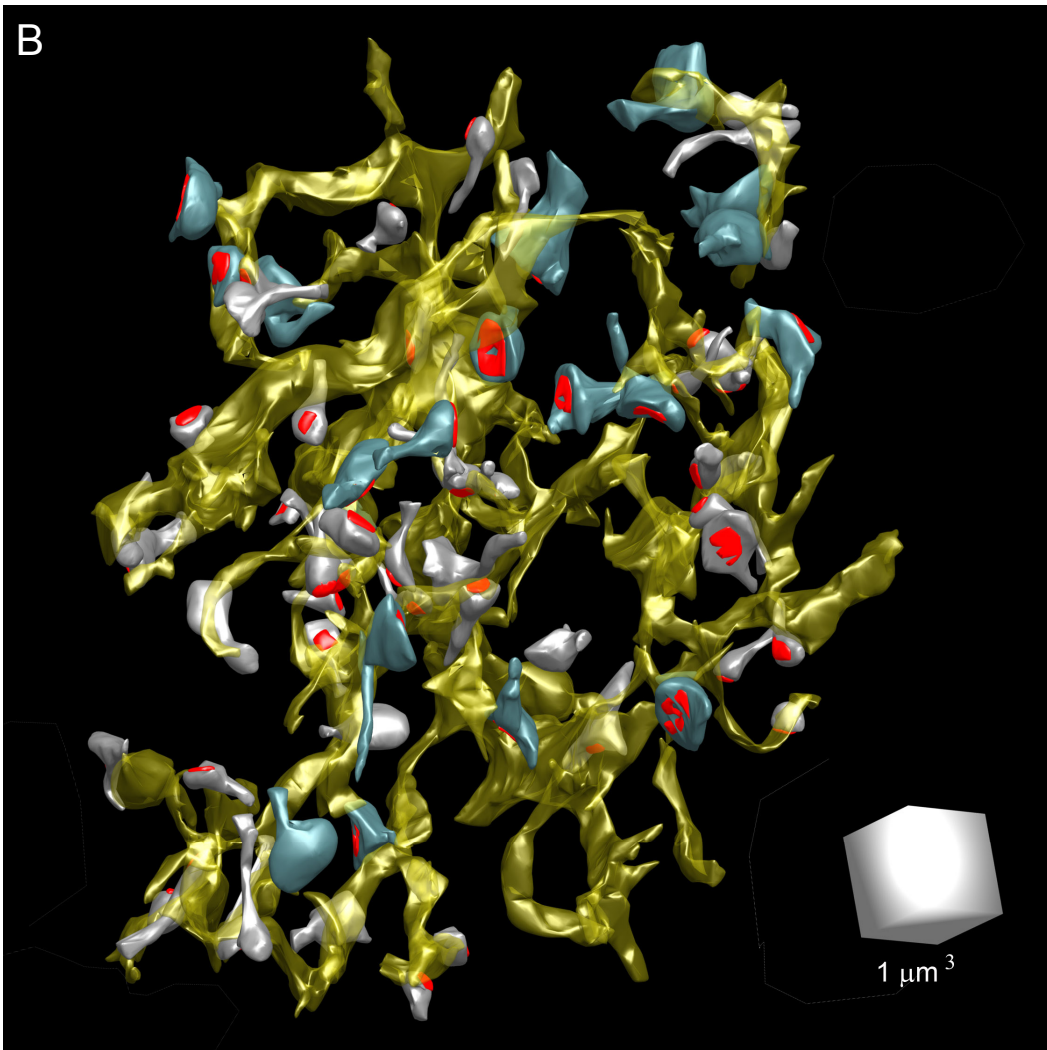
Figure S3. An example of serial sections which include profiles of the astrocyte recorded and labelled in an acute slice. Related to Fig. 3.

(A) Eight (1-8) 60 nm thick adjacent serial sections are shown, as indicated with areas depicting dendritic spines (yellow; sp1-sp5) and astroglia (blue, filled with electron dense particles resulting from DAB conversion of the recorded astrocyte filled with biocytine; ast); scale bar, 500 nm.

(B) An example of the 3D reconstruction depicting an astrocyte fragment (yellow, colors reversed compared to A with adjacent postsynaptic spines (bluish grey) equipped with postsynaptic densities (red).

(C) The average areas of astroglial surfaces (mean ± SEM; rendered from 3D reconstruction of aligned sections; Methods Details) within 100 nm- thick 3D concentric shells centered at the postsynaptic density of individual dendritic spines, before and 20-25 min after LTP, as indicated. Two types of spines are shown; n, spine numbers analyzed; ***, $p < 0.001$; see Fig. 3 for further detail and illustrations.
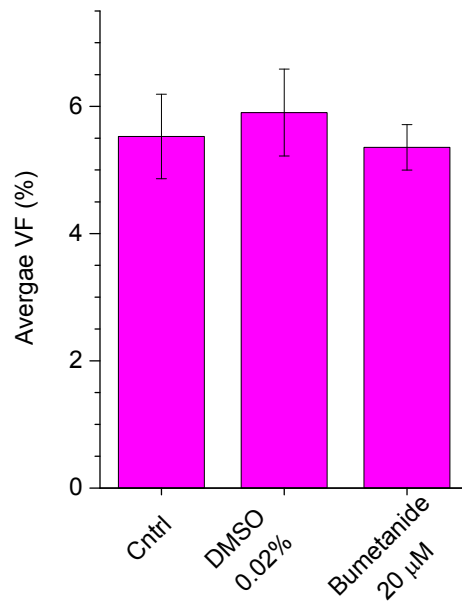
Figure S4. Bumetanide (or vehicle DMSO) have no baseline effect on the astroglial volume. Related to Fig. 4.

Astroglial volume fraction (mean ± SEM) measured in control conditions (Cntrl, 5.52 ± 0.66; n = 14), with the vehicle 0.02% DMSO (5.90 ± 0.68; n = 8), and with 20 μM bumetanide inside the cell (5.35 ± 0.36; n = 19)
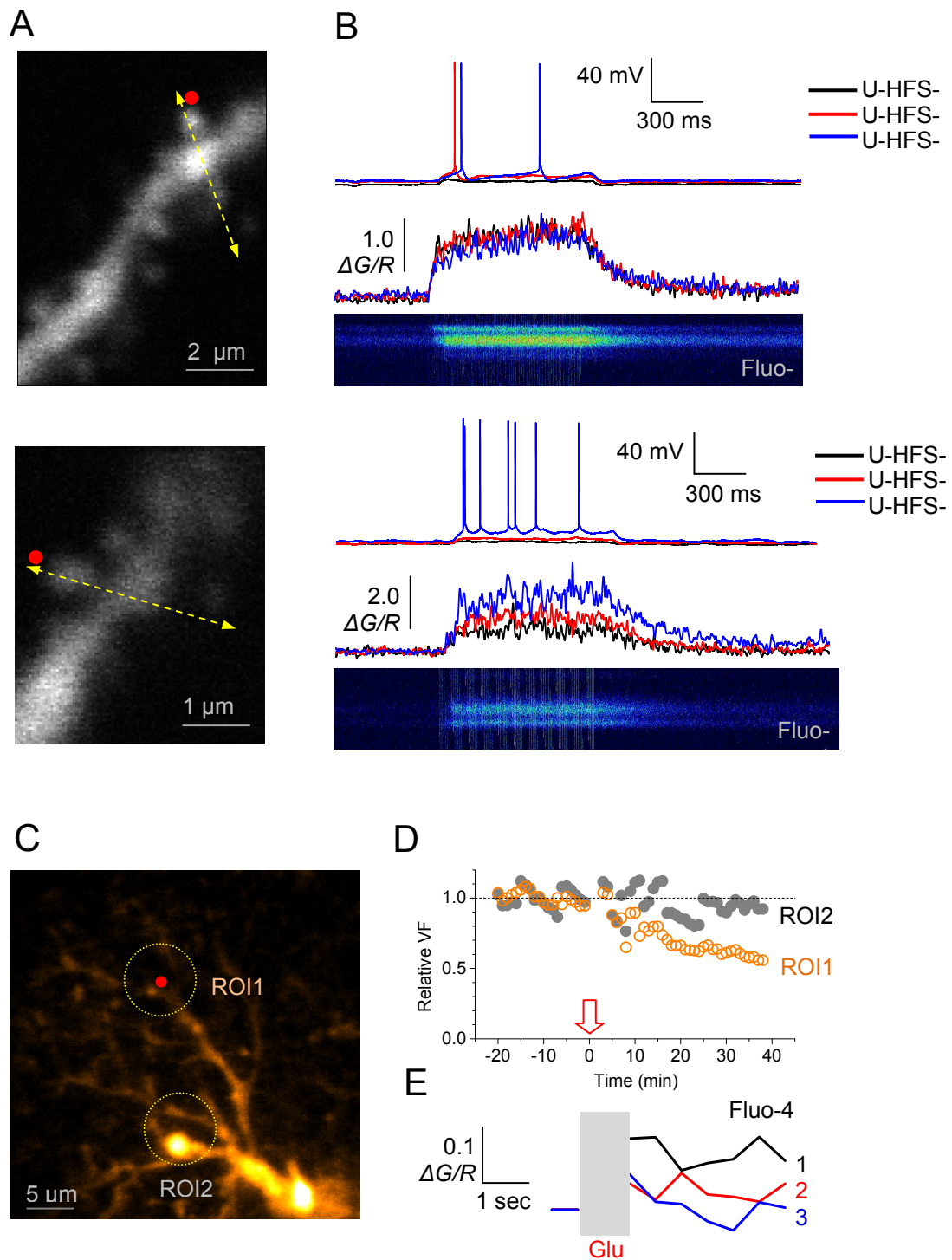
Figure S5. Spot-uncaging of MNI-glutamate near dendritic spines (LTP induction protocol) induces substantial postsynaptic depolarization and Ca²⁺ entry while reducing local volume fraction (VF) of astroglia: individual cell examples. Related to Fig. 5.

(A) Alexa Fluo 594 channel showing dendritic fragments (including spines) from two example CA1 pyramidal cells. Red dot, 2P MNI-glutamate uncaging spot; yellow arrow, linescan position; cells are held in whole-cell current-clamp mode (at -60...65 mV in

baseline conditions); MNI-glutamate uncaging at λ_U^{2P} = 720 nm; Alexa imaging at λ_x^{2P} = 840 nm.

(B) Somatic voltage recording (upper traces) and postsynaptic Ca^{2+}-sensitive linescan recording (lower traces, $\Delta G/R$; linescan, Fluo-4 channel) during the three trains of 2P-uncaging pulses in the LTP induction protocol (100 x 1 ms laser pulses at 100Hz, three series 60 s apart; uncaging pulse bleed-through trace can be seen in linescans), as indicated by color (three traces superimposed) and notations U-HFS-1/2/3, respectively. Intermittent spikes can be seen in some traces.

(C) An astrocyte fragment (averaged 9-section z-stack) depicting the uncaging spot (red dot) and two regions of interest (ROIs) for VF measurement; Alexa Fluor 594 channel.

(D) Time course of the relative VF in the two ROIs (ROI1 and ROI2) indicated in C. Red arrow, the onset of LTP induction protocol using 2P spot-uncaging of MNI glutamate (one hundred of 1 ms pulses at 100 Hz, three series 1 min apart; Method Details).

(E) Time course of Ca^{2+}-sensitive fluorescence averaged within ROI1 before and immediately after 2P spot-uncaging (grey area), for each of the three series of pulses (indicated 1, 2, 3). Further illustrations are in Fig. 5E-F.
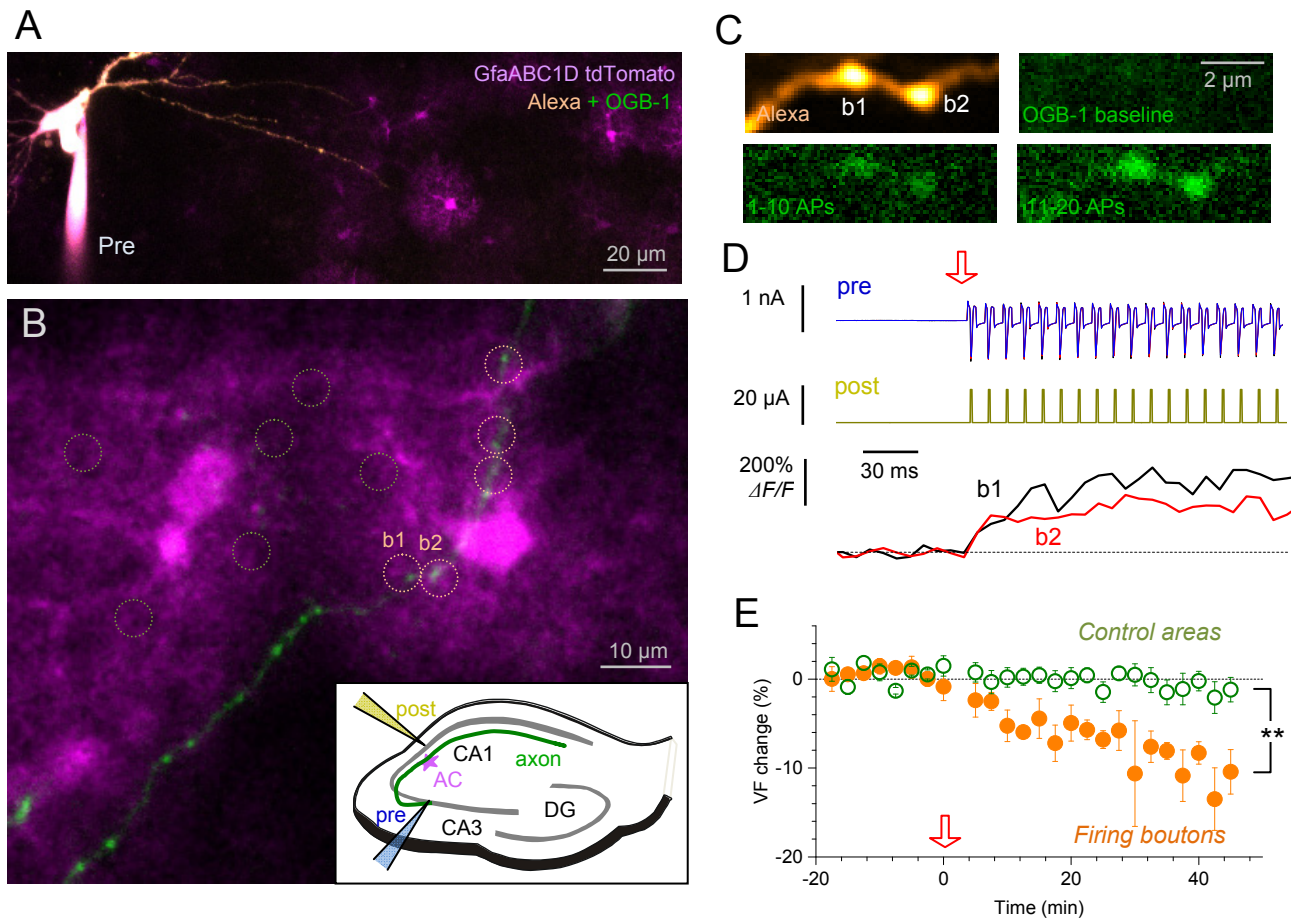
Figure S6. LTP pairing protocol for a single CA3 pyramidal cell axon leads to astroglial withdrawal near active axonal boutons. Related to Fig. 6.

(A) CA3 pyramidal cell shown held in whole-cell (dialyzed with 50 µM Alexa 594 and 200 µM OGB-1), with the axon proximal part seen traced into the field of astrocytes labelled with tdTomato (magenta); a 67 µm deep z-stack projection image (two-laser 2PE at λ_x^{2p} = 800 nm and λ_x^{2p} = 910 nm).

(B) A distal fragment of the axon (green) which originates from the cell shown in (A) and trespasses local astroglia (magenta); orange dotted circles, ROIs for astroglial VF analyses near five firing presynaptic boutons (see below for Ca^{2+} recordings in boutons b1 and b2); green dotted circles, examples of control astroglial areas devoid of the presynaptic axon. Inset, experiment diagram of LTP induction protocol by pairing, depicting presynaptic cell held in whole-cell (as in A), a postsynaptic stimulating electrode placed in *s. pyramidale* (yellow; to depolarize / fire postsynaptic cells), a single traced axon (green) trespassing an astrocyte (AC, magenta); a 67 µm deep z-stack projection image for two-laser 2PE as in A.

(C) Examples of two presynaptic axonal boutons (b1 and b2 in B), shown in the Alexa channel (red) and in the Ca^{2+} sensitive OGB-1 channel (green) in baseline conditions and following the initial burst of presynaptic action potentials 1-10, and 11-20 (at 100 Hz), as indicated.

(D) Examples of presynaptic whole-cell electrode recordings (blue, individual evoked spikes shown), postsynaptic extracellular electrode pulse control (dark yellow), and OGB-1 fluorescence in boutons b1 and b2 (shown in B-C), in the initial phase of the LTP induction protocol (3 x 1 s trains @ 100 Hz; red arrow, onset).

(E) Time course of astroglial VF changes (mean ± SEM) near firing axonal boutons (orange dots, the corresponding ROIs shown by orange circles in B; n = 5) and in control areas (ROI examples shown by green circles in B; n = 10) before and after the LTP induction protocol (red arrow); **, $p < 0.01$ (two-samples t-test for 25-45 min interval post-induction); the data were routinely adjusted to account for the (small) experiment-wide tdTomato photobleaching given by $P(t) = 0.9723 + 0.00867 \, e^{-t/\tau}$ with τ = 10.9 min.
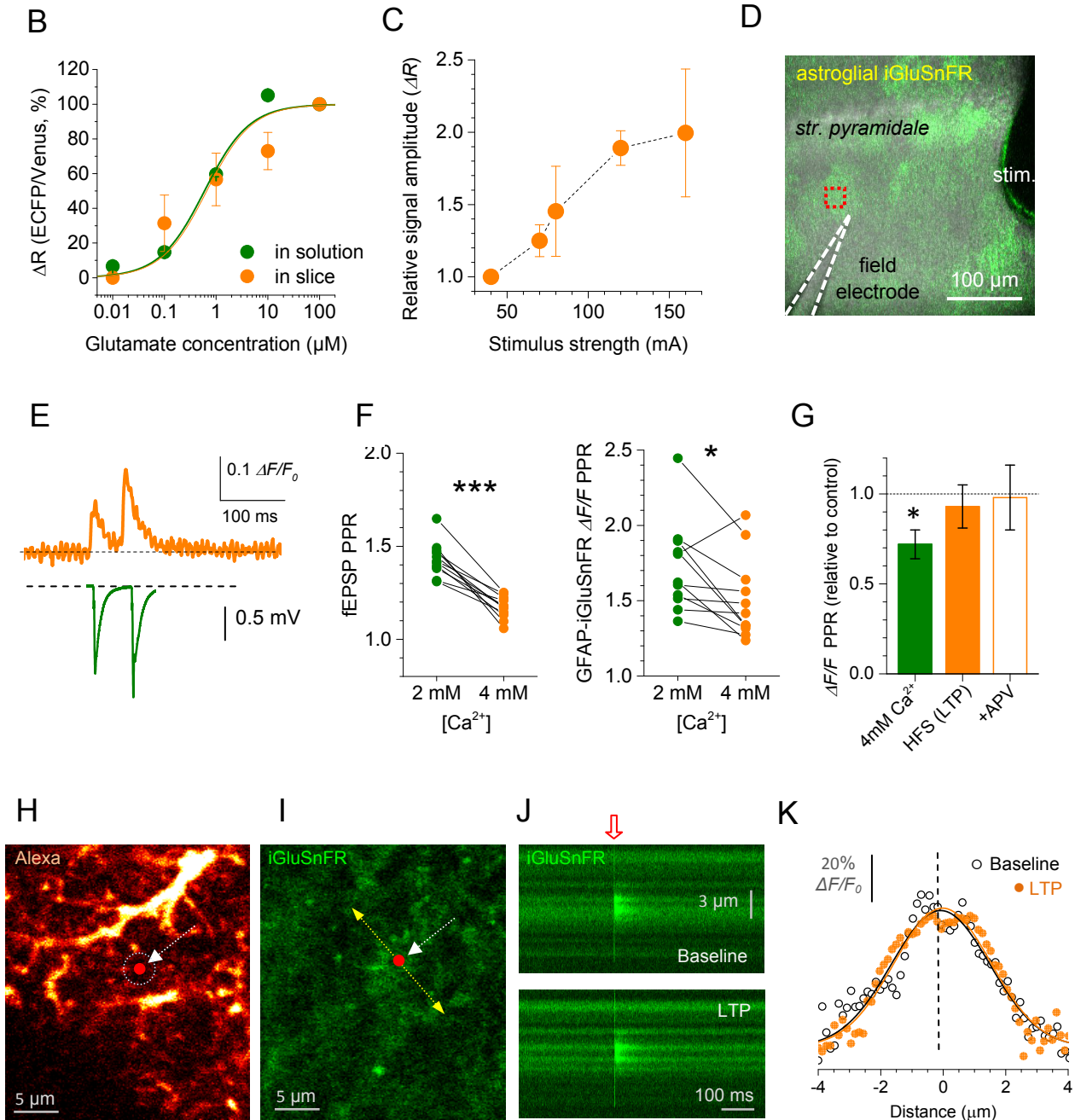
A

DNA:

ATCTCGATCCCGCGAAATTAATACGACTCACTATAGGGAGACCACAACGGTTTCCCTCTAGATAATTTTGTTTAACTTTAAGAAGGAGATATACATATGCGGGGTTCTCAT
CATCATCATCATCATGGTATGGCTAGCATGACTGGTGGACAGCAAATGGGTCGGGATCTGTACGACGATGACGATAAGGATCCGAAACTGAAGGTAACAGTCAACGGCACT
GCGTATGACGTTGACGTCGACAAGTCACACGAAAACCCGATGGGCACCATCCTGTTCGGCGGCGGCACCGGCGGCGCGCCGGCACCGGCAGCAGGTGGCGCAGGC
GCCGGTAAGGCCGGAGAGGGCGAGATTCCCGCTCCGCTGGCCGGCACCGTCTCCAAGATCCTCGTGAAGGAGGGTGACACGGTCAAGGCTGGTCAGACCGTGCTCGTTCTC
GAGGCCATGAAGATGGAGACCGAGATCAACGCTCCCACCGACGGCAAGGTCGAGAAGGTCCTGGTCAAGGAGCGTGACGCGGTGCAGGGCGGTCAGGGTCTCATCAAGATC
GGGGATCTCGAGCTCATCGAAGGCTCGAGCGGTTCGGATCCGGGCCGCATGGTGAGCAAGGGCGAGGAGCTGTTCACCGGGGTGGTGCCCATCCTGGTCGAGCTGGACGGC
GACGTAAACGGCCACAAGTTCAGCGTGTCCGGCGAGGGCGAGGGCGATGCCACCTACGGCAAGCTGACCCTGAAGTTCATCTGCACCACCGGCAAGCTGCCCGTGCCCTGG
CCCACCCTCGTGACCACCCTGACCTGGGGCGTGCAGTGCTTCAGCCGCTACCCCGACCACATGAAGCAGCACGACTTCTTCAAGTCCGCCATGCCCGAAGGCTACGTCCAG
GAGCGCACCATCTTCTTCAAGGACGACGGCAACTACAAGACCCGCGCCGAGGTGAAGTTCGAGGGCGACACCCTGGTGAACCGCATCGAGCTGAAGGGCATCGACTTCAAG
GAGGACGGCAACATCCTGGGGCACAAGCTGGAGTACAACTACATCAGCCACAACGTCTATATCACCGCCGACAAGCAGAAGAACGGCATCAAGGCCAACTTCAAGATCCGC
CACAACATCGAGGACGGCAGCGTGCAGCTCGCCGACCACTACCAGCAGAACACCCCCATCGGCGACGGCCCCGTGCTGCTGCCCGACAACCACTACCTGAGCACCCAGTCC
GCCCTGAGCAAAGACCCCAACGAGAAGCGCGATCACATGGTCCTGCTGGAGTTCGTGACCGCCGCCGGGATCACTCTCGGCATGGACGAGCTGTACAAGGGTGGTACCGGA
GGCGCCGCAGGCAGCACGCTGGACAAAATCGCCAAAAACGGTGTGATTGTCGTCGGTCACCGTGAATCTTCAGTGCCTTTCTCTTATTACGACAATCAGCAAAAGTGGTG
GGTTACTCGCAGGATTACTCCAACGCCATTGTTGAAGCAGTGAAAAAGAAACTCAACAAACCGGACTTGCAGGTAAAACTGATTCCGATTACCTCACAAAACCGTATTCCA
CTGCTGCAAAACGGCACTTTCGATTTTGAATGTGGTTCTACCACCAACAACGTCGAACGCCAAAAACAGGCGGCTTTCTCTGACACTATTTTCGTGGTCGGTACGCGCCTG
TTGACCAAAAAGGGTGGCGATATCAAAGATTTTGCCAACCTGAAAGACAAAGCCGTAGTCGTCACTTCCGGCACTACCTCTGAAGTTTTGCTCAACAAACTGAATGAAGAG
CAAAAAATGAATATGCGCATCATCAGCGCCAAAGATCACGGTGACTCTTTCCGCACCCTGGAAAGCGGTCGTGCCGTTGCCTTTATGATGGATGACGCTCTGCTGGCCGGT
GAACGTGCGAAAGCGAAGAAACCAGACAACTGGGAAATCGTCGGCAAGCCGCAGTCTCAGGAGGCCTACGGTTGTATGTTGCGTAAAGATGATCCGCAGTTCAAAAAGCTG
ATGGATGACACCATCGCTCAGGTGCAGACCTCCGGTGAAGCGGAAAAATGGTTTGATAAGTGGTTCAAAAATCCAATTCCGCCGAAAAACCTGAACATGAATTTCGAACTG
TCAGACGAAATGAAAGCACTGTTCAAAGAACCGAATGACAAGGCACTGAACGGCGCCGGTACCGGTGGAATGGTGAGCAAGGGCGAGGAGCTGTTCACCGGGGTGGTGCCC
ATCCTGGTCGAGCTGGACGGCGACGTAAACGGCCACAAGTTCAGCGTGTCCGGCGAGGGCGAGGGCGATGCCACCTACGGCAAGCTGACCCTGAAGCTGATCTGCACCACC
GGCAAGCTGCCCGTGCCCTGGCCCACCCTCGTGACCACCCTGGGCTACGGCCTGCAGTGCTTCGCCCGCTACCCCGACCACATGAAGCAGCACGACTTCTTCAAGTCCGCC
ATGCCCGAAGGCTACGTCCAGGAGCGCACCATCTTCTTCAAGGACGGCAACTACAAGACCCGCGCCGAGGTGAAGTTCGAGGGCGACACCCTGGTGAACCGCATCGAG
CTGAAGGGCATCGACTTCAAGGAGGACGGCAACATCCTGGGGCACAAGCTGGAGTACAACTACAACAGCCACAACGTCTATATCACCGCCGACAAGCAGAAGAACGGCATC
AAGGCCAACTTCAAGATCCGCCACAACATCGAGGACGGCGGCGTGCAGCTCGCCGACCACTACCAGCAGAACACCCCCATCGGCGACGGCCCCGTGCTGCTGCCCGACAAC
CACTACCTGAGCTACCAGTCCGCCCCTGAGCAAAGACCCCAACGAGAAGCGCGATCACATGGTCCTGCTGGAGTTCGTGACCGCCGCCGGGATCACTCTCGGCATGGACGAG
CTGTACAAGTAAAAGCTTGATCCGGCTGCTAACAAAGCCCGAAAGGAAGCTGAGTTGGCTGCTGCCACCGCTGAGCAATAACTAGCATAACCCCTTGGGGCCTCTAAACGG
GTCTTGAGGGGTTTTTTGCTGAAAGGAGGAACTATATCCGGATCTGGCGTAATAGCGAAGAGGCCCGCACCGATCGCCCTTCCCAACAGTTGCGCAGCCTGAATGGCGAAT
GGGACGCGCCCTGTAGCGGCGCATTAAGCGCGGCGGGTGTGGTGGTTACGCGCAGCGTGACCGCTACACTTGCCAGCGCCCTAGCGCCCGCTCCTTTCGCTTTCTTCCCTT
CCTTTCTCGCCACGTTCGCCGGCTTTCCCCGTCAAGCTCTAAATCGGGGGCTCCCTTTAGGGTTCCGATTTAGAGCTTTACGGCACCTCGACCGCAAAAAACTTGATTTGG
GTGATGGTTCACGTAGTGGGCCATCGCCCTGATAGACGGTTTTTCGCCCTTTGACGTTGGAGTCCACGTTCTTTAATAGTGGACTCTTGTTCCAAACTGGAACAACACTCA
ACCCTATCGCGGTCTATTCTTTTGATTTATAAGGGATTTTGCCGATTTCGGCCTATTGGTTAAAAAATGAGCTGATTTAACAAATATTTAACGCGAATTTTAACAAAATAT
TAACGTTTACAATTTCGCCTGATGCGGTATTTTCTCCTTACGCATCTGTGCGGTATTTCACACCGCATACAGGTGGCACTTTTCGGGGAAATGTGCGCGGAACCCCTATTT
GTTTATTTTTCTAAATACATTCAAATATGTATCCGCTCATGAGACAATAACCCTGATAAATGCTTCAATAATATTGAAAAAGGAAGAGTATGAGTATTCAACATTTCCGTG
TCGCCCTTATTCCCTTTTTTGCGGCATTTTGCCTTCCTGTTTTTGCTCACCCAGAAACGCTGGTGAAAGTAAAAGATGCTGAAGATCAGTTGGGTGCACGAGTGGGTTACA
TCGAACTGGATCTCAACAGCGGTAAGATCCTTGAGAGTTTTCGCCCCGAAGAACGTTTTCCAATGATGAGCACTTTTAAAGTTCTGCTATGTGATACACTATTATCCCGTA
TTGACGCCGGGCAAGAGCAACTCGGTCGCCGCATACACTATTCTCAGAATGACTTGGTTGAGTACTCACCAGTCACAGAAAAGCATCTTACGGATGGCATGACAGTAAGAG
AATTATGCAGTGCTGCCATAACCATGAGTGATAACACTGCGGCCAACTTACTTCTGACAACGATCGGAGGACCGAAGGAGCTAACCGCTTTTTTGCACAACATGGGGGATC
ATGTAACTCGCCTTGATCGTTGGGAACCGGAGCTGAATGAAGCCATACCAAACGACGAGAGTGACACCACGATGCCTGTAGCAATGCCAACAACGTTGCGCAAACTATTAA
CTGGCGAACTACTTACTCTAGCTTCCCGGCAACAATTAATAGACTGAATGGAGGCGGATAAAGTTGCAGGACCACTTCTGCGCTCGGCCCTTCCGGCTGGCTGGTTTATTG
CTGATAAATCTGGAGCCGGTGAGCGTGGGTCTCGCGGTATCATTGCAGCACTGGGGCCAGATGGTAAGCGCTCCCGTATCGTAGTTATCTACACGACGGGGAGTCAGGCAA
CTATGGATGAACGAAATAGACAGATCGCTGAGATAGGTGCCTCACTGATTAAGCATTGGTAACTGTCAGACCAAGTTTACTCATATATACTTTAGATTGATTTAAAACTTC
ATTTTTAATTTAAAAGGATCTAGGTGAAGATCCTTTTTGATAATCTCATGACCAAAATCCCTTAACGTGAGTTTTCGTTCCACTGAGCGTCAGACCCCGTAGAAAAGATCA
AAGGATCTTCTTGAGATCCTTTTTTTCTGCGCGTAATCTGCTGCTTGCAAACAAAAAAACCACCGCTACCAGCGGTGGTTTGTTTGCCGGATCAAGAGCTACCAACTCTTT
TTCCGAAGGTAACTGGCTTCAGCAGAGCGCAGATACCAAATACTGTCCTTCTAGTGTAGCCGTAGTTAGGCCACCACTTCAAGAACTCTGTAGCACCGCCTACATACCTCG
CTCTGCTAATCCTGTTACCAGTGGCTGCTGCCAGTGGCGATAAGTCGTGTCTTACCGGGTTGGACTCAAGACGATAGTTACCGGATAAGGCGCAGCGGTCGGGCTGAACGG
GGGGTTCGTGCACACAGCCCAGCTTGGAGCGAACGACCTACACCGAACTGAGATACCTACAGCGTGAGCTATGAGAAAGCGCCACGCTTCCCGAAGGGAGAAAGGCGGACA
GGTATCCGGTAAGCGGCAGGGTCGGAACAGGAGAGCGCACGAGGGAGCTTCCAGGGGGAAACGCCTGGTATCTTTATAGTCCTGTCGGGTTTCGCCACCTCTGACTTGAGC
GTCGATTTTTGTGATGCTCGTCAGGGGGGCGGAGCCTATGGAAAAACGCCAGCAACGCGGCCTTTTTACGGTTCCTGGCCTTTTGCTGGCCTTTTGCTCACATGTTCTTTC
CTGCGTTATCCCCTGATTCTGTGGATAACCGTATTACCGCCTTTGAGTGAGCTGATACCGCTCGCCGCAGCCGAACGACCGAGCGCAGCGAGTCAGTGAGCGAGGAAGCGG
AAGAGCGCCCAATACGCAAACCGCCTCTCCCCGCGCGTTGGCCGATTCATTAATGCAG

Protein:

MRGSHHHHHHGMASMTGGQQMGRDLYDDDDKDPKLKVTVNGTAYDVDVDVDKSHENPMGTILFGGGTGGAPAPAAGGAGAGKAGEGEIPAPLAGTVSKILVKEGDTVKAGQ
TVLVLEAMKMETEINAPTDGKVEKVLVKERDAVQGGQGLIKIGDLELIEGSSGSDPGRMVSKGEELFTGVVPILVELDGDVNGHKFSVSGEGEGDATYGKLTLKFICTTGK
LPVPWPTLVTTLTWGVQCFSRYPDHMKQHDFFFKSAMPEGYVQERTIFFKDDGNYKTRAEVKFEGDTLVNRIELKGIDFKEDGNILGHKLEYNYISHNVYITADKQKNGIKA
NFKIRHNIEDGSVQLADHYQQNTPIGDGPVLLPDNHYLSTQSALSKDPNEKRDHMVLLEFVTAAGITLGMDELYKGGTGGAAGSTLDKIAKNGVIVVGHRESSVPFSYYDN
QQKVVGYSQDYSNAIVEAVKKKLNKPDLQVKLIPITSQNRIPLLQNGTFDFECGSTTNNVERQKQAAFSDTIFVVGTRLLTKKGGDIKDFANLKDKAVVVTSGTTSEVLLN
KLNEEQKMNMRIISAKDHGDSFRTLESGRAVAFMMDDALLAGERAKAKKPDNWEIVGKPQSQEAYGCMLRKDDPQFKKLMDDTIAQVQTSGEAEKWFDKWFKNPIPPKNLN
MNFELSDEMKALFKEPNDKALNGAGTGGMVSKGEELFTGVVPILVELDGDVNGHKFSVSGEGEGDATYGKLTLKLICTTGKLPVPWPTLVTTLGYGLQCFARYPDHMKQHD
FFFKSAMPEGYVQERTIFFKDDGNYKTRAEVKFEGDTLVNRIELKGIDFKEDGNILGHKLEYNYNSHNVYITADKQKNGIKANFKIRHNIEDGGVQLADHYQQNTPIGDGPV
LLPDNHYLSYQSALSKDPNEKRDHMVLLEFVTAAGITLGMDELYK-

Figure S7. Monitoring extrasynaptic glutamate escape with optical glutamate sensors bFLIPE600n and iGluSnFR. Related to Fig. 7.

(A) Glutamate sensor bFLIPE600n: DNA and protein sequences. Functionally relevant parts are color coded, as follows: His-tag, Biotin-tag, ECFP, flexible linker (GSSG) after biotin tag, GltI, Venus.

(B) Monitoring glutamate sensitivity of bFLIPE600n immobilized in acute hippocampal slices. Glutamate levels were estimated by calculating the fluorescence intensity ratio R

= ECFP/Venus and its changes (ΔR). Titration of bFLIPE600n was performed in free solution and acute slices (ΔR versus nominally zero glutamate; free solution: Kd = 596 nM, n = 3; acute slices Kd = 659 nM, n = 5). *In situ* measurements were performed in the presence of 10 µM NBQX, 50 µM D-APV, 1 µM TFB-TBOA, 1 µM TTX, 50 µM LY341495. Calibration curves, Hill equation approximation (Hill coefficient set to one).

(C) The input-output evaluation bFLIPE600n sensitivity: glutamate transient amplitude versus stimulation intensity (mean ± SEM, n = 4) in CA1 *s.radiatum*; ΔR signal is normalized to the baseline response at 40 µA stimulus.

(D) Glutamate sensor iGluSnFR expressed on astrocytic membranes in CA1 *s. radiatum* (Method details), shown with a stimulating (stim) and recording field electrode; boxed area, fluorescence imaging area.

(E) iGluSnFR fluorescence intensity traces ($\Delta F/F_0$) in response to paired-pulse stimuli (*top*, 50 ms apart, average of 100 trials) faithfully reflect fEPSPs recorded in parallel (*bottom*).

(F) Paired-pulse experiments (as in E) showing that increasing extracellular [Ca^{2+}] reduces paired-pulse ratio (PPR) for both fEPSPs (left; p < 0.001) and optical iGluSnFR responses (right; p = 0.019; n = 11; paired *t*-tests).

(G) HFS-induced LTP (n = 13) or HFS in the presence of 50 µM APV (n = 5) have no effect on the paired-pulse ratio (PPR) of iGluSnFR responses whereas increasing extracellular [Ca^{2+}] to 4 mM reduces PPR (n = 11) of optical iGluSnFR signal (as in F).

(H) A fragment of astrocyte held in whole-cell mode (Alexa Fluor 594 channel, λ_x^{2P} = 910 nm; single optical section) illustrating the LTP induction protocol with spot-uncaging of glutamate (red dot, arrow; λ_u^{2P} = 720 nm); intracellular solution contains 100 µM Alexa Fluor 594 and 20 µM bumetanide; dotted circle, ROI for monitoring local tissue volume fraction (VF) of astroglia during LTP induction. See Figure 4H for statistical summary.

(I) Fragment in H shown in the iGluSnFR channel (λ_x^{2P} = 910 nm); arrow, linescan positioning; red dot, spot-uncaging location (as in H).

(J) Examples of linescan traces (position shown in I) recorded before and ~20 min after LTP the induction spot-uncaging protocol (baseline and LTP, respectively).

(K) Examples of the spatial glutamate-sensitive iGluSnFR fluorescence profiles (dots, individual pixel values) evoked by a 1 ms glutamate uncaging pulse, before (Baseline) and 20-25 min after LTP induction, as indicated, in the experiment illustrated in I-J; zero abscissa, the uncaging spot position (red dot in I); black and orange solid lines, best-fit Gaussian approximation; see Figure 5I for statistical summary.
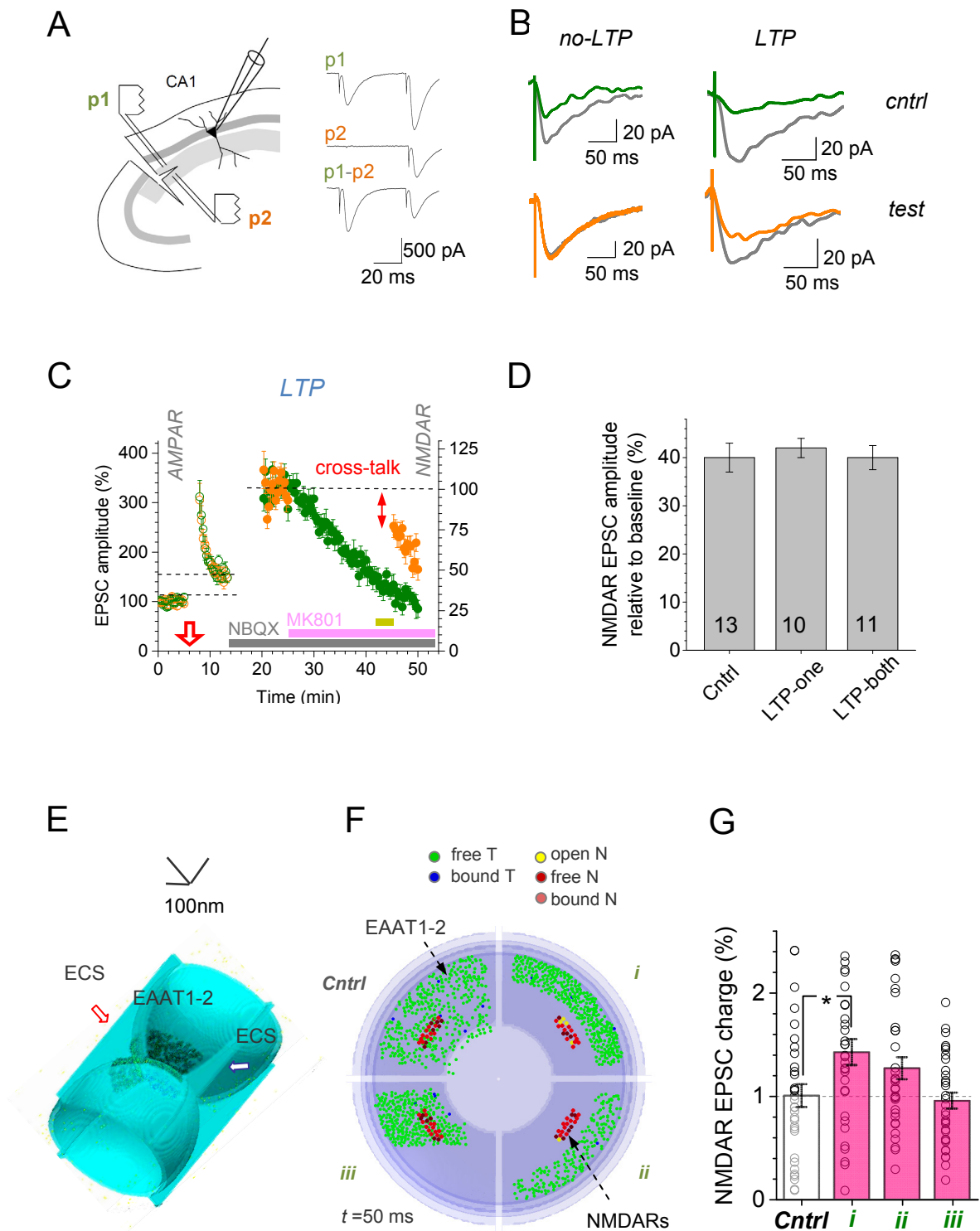
Figure S8. Electrophysiological probing of NMDAR-mediated inter-synaptic cross-talk and a biophysical plausibility test. Related to Fig. 8.

(A) *Diagram*, a previously established test (Scimemi et al., 2004) for presynaptic independence of two Schaffer collateral pathways (p1 and p2) converging onto a CA1 pyramidal cell. *Traces*, EPSCs show paired-pulse facilitation during p1-p1 stimulation but not across the pathways (p1-p2, modified from (Scimemi et al., 2004)). In the recorded sample (*n* = 54 slices), paired-pulse facilitation with a 50 ms interval was 75.4 ± 6.1 % (*P* < 0.001) in the same pathway and only 16.5 ± 2.9% across (difference at p < 0.001).

(B) Characteristic one-cell examples (experiments summarized in Fig. 8A-B) of NMDAR EPSCs recorded in baseline conditions (grey) and during resumption of stimulation in control (*cntrl*, green) and test (orange) pathways, in baseline conditions (*no-LTP*) and with LTP induced prior to the cross-talk test (*LTP*).

(C) The summary of two-pathway experiments similar to those shown Fig. 8A, but with LTP induced simultaneously in both (rather than one) afferent pathways. Notations are as in Fig. 8A; yellow-green segment, period over which the degree of NMDAR EPSC suppression by MK801, prior to the resumption of silent pathway stimulation, was measured.

(D) The reduction of the NMDAR EPSC amplitude (mean ± SEM, sample size n shown) following application of MK801, prior to the resumption of test pathway stimulation (averaging time interval depicted by yellow segment), in experiments with no LTP, with LTP induced in the control pathway (LTP-one), and with LTP induced in both pathways (LTP-both). See Fig. 8A for the corresponding time course data. Similar values of the MK801-induced decay in the three conditions indicate similar release probabilities in the bulk of stimulated synapses, with or without LTP induction.

(E) A 3D Monte-Carlo model of the CA3-CA1 synapse, with the pre- and postsynaptic truncated hemispheres (separated by the synaptic cleft), extracellular space gaps (ECS) and transporter clusters (EAAT1-2) shown (Method details) as detailed and tested earlier (Zheng et al., 2008).

(F) Front view (cross-section) of the model shown in A. Four simulated scenarios of astroglial EAAT1 changes (green dot scatter) during LTP are depicted, in four different quadrants: *Cntrl* (random scatter), *i* (even withdrawal, same transporter numbers), *ii* (even withdrawal, same transporter density. ~50% drop in numbers), *and iii* (withdrawal to one side, same transporter numbers). Images illustrate a snapshot of NMDAR activation 50 ms following release of 3000 glutamate molecules from the center; EAAT1 transporter (T) and NMDAR (N) states are color-coded, as indicated.

(G) Summary of Monte Carlo experiments (n = 32 runs) shown in E-F. Average NMDAR-mediated charge transfer relative to Control (*Cntrl*), for the three types of change: *i* (1.42 ± 0.13, p < 0.015 compared to control), *ii* (1.26 ± 0.11), and *iii* (0.95 ± 0.08); dots, data points at individual runs; note high variability due to a few NMDARs being activated stochastically per release. The data indicate that scenario *i* is most likely

to correspond to the larger increase in extrasynaptic NMDAR activation after LTP induction.

Supplementary References

Nolte, C., Matyash, M., Pivneva, T., Schipke, C.G., Ohlemeyer, C., Hanisch, U.K., Kirchhoff, F., and Kettenmann, H. (2001). GFAP promoter-controlled EGFP-expressing transgenic mice: a tool to visualize astrocytes and astrogliosis in living brain tissue. Glia *33*, 72-86.

Scimemi, A., Fine, A., Kullmann, D.M., and Rusakov, D.A. (2004). NR2B-containing receptors mediate cross talk among hippocampal synapses. J. Neurosci. *24*, 4767-4777.

Zheng, K., Scimemi, A., and Rusakov, D.A. (2008). Receptor actions of synaptically released glutamate: the role of transporters on the scale from nanometers to microns. Biophys J *95*, 4584-4596.